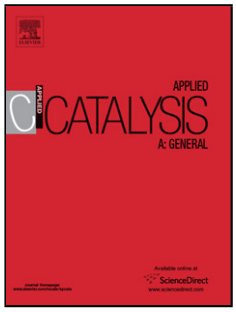

Title: Iron exchanged tungstophosphoric acid supported on activated carbon derived from pinecone biomass: Evaluation of catalysts efficiency for liquid phase benzylation of anisole with benzyl alcohol

Author: Chowdari Ramesh Kumar N. Rambabu K.C. Maheria A.K. Dalai N. Lingaiah

PII: S0926-860X(14)00464-5
DOI: http://dx.doi.org/doi:10.1016/j.apcata.2014.07.034
Reference: APCATA 14927

To appear in: *Applied Catalysis A: General*

Received date: 15-10-2013
Revised date: 23-7-2014
Accepted date: 28-7-2014

Please cite this article as: C.R. Kumar, N. Rambabu, K.C. Maheria, A.K. Dalai, N. Lingaiah, Iron exchanged tungstophosphoric acid supported on activated carbon derived from pinecone biomass: Evaluation of catalysts efficiency for liquid phase benzylation of anisole with benzyl alcohol, *Applied Catalysis A, General* (2014), http://dx.doi.org/10.1016/j.apcata.2014.07.034

Iron exchanged tungstophosphoric acid supported on activated carbon derived from pinecone biomass:

Evaluation of catalysts efficiency for liquid phase benzylation of anisole with benzyl alcohol

Chowdari Ramesh Kumar[1, 2], N. Rambabu[1], K.C. Maheria[1, 3], A.K. Dalai[1*], and N. Lingaiah[2]

[1]*Department of Chemical and Biological Engineering, University of Saskatchewan, Saskatoon, SK–S7N 5A9, Canada*

[2]*Catalysis Laboratory, Inorganic & Physical Chemistry Division, CSIR–Indian Institute of Chemical Technology, Hyderabad–500 007, Telangana, India*

[3] *Department of Applied Chemistry, S.V. National Institute of Technology, Ichchhanath, Surat–395 007, Gujarat, India*

Submitted for publication in:
Applied Catalysis A: General

Corresponding author:
Dr. Ajay K. Dalai,
University of Saskatchewan
57 Campus Drive
Saskatoon, SK Canada S7N 5A9
Email: ajay.dalai@usask.ca
Phone No. (306) 966-4771
Fax No. (306) 966-4777
http://www.engr.usask.ca/~dalai

Highlights

- Synthesized the Iron exchanged TPA supported on pinecone activated carbon catalysts.
- Investigated the optimum dosage of TPA–Fe loading for higher conversion.
- Evaluated the effects of activated carbon porous structure and acidity on benzylation reaction.
- Effective and optimum conditions were investigated for benzylation reaction.

Abstract

A series of iron–exchanged heteropoly tungstate (TPA–Fe) supported on activated carbon produced from pinecone biomass, have been investigated as catalysts for the benzylation reaction. Catalysts were characterized by FT–IR, XRD, Laser Raman, BET surface area, and ammonia TPD analysis. FT–IR, XRD, and Raman data revealed retention of the Keggin ion on activated carbon–supported catalysts. The catalytic activity of these catalysts was evaluated for liquid phase benzylation of anisole with benzyl alcohol. The catalytic activity was significantly dependent on the dispersion of TPA–Fe on activated carbon. The effect of TPA–Fe loading on activated carbon was studied ranging from 40 to 80 wt%. The catalyst with 70 wt% loading of TPA–Fe showed higher benzylation activity, which is related to variation in acidity of the catalysts. Thermal stability and structural properties of the catalysts were studied by treating the catalyst at different calcination temperatures. The benzyl alcohol conversion and selectivity towards benzylated products were also dependent on the anisole to benzyl alcohol molar ratio,

reaction temperature, and catalyst concentration/loading. To know the effect of the benzylating agent, the reaction was carried out using benzyl chloride, benzyl alcohol, and dibenzylether. The preferential order for conversion of the benzylating agent was observed as benzyl chloride > benzyl alcohol > dibenzylether. This study indicated that biomass derived activated carbon is suitable support to disperse Keggin type heteropoly acid for the benzylation reaction.

Key words: Activated carbon, Benzylation, Heteropoly tungstate, Keggin ion, Pinecone

1 Introduction

Alkylation of aromatic compounds is a very important reaction since diphenylmethane and substituted diphenylmethane compounds are versatile chemical feedstocks for a wide range of industrial products such as benzophenone, substituted benzophenone, 2–/4–nitrodiphenylmethane, diamines of diphenylmethane and diphenylmethanes which are used as monomers for poly carbonate resins, aromatic solvents, pharmaceuticals, dyes, perfumes [1]. Synthesis of these compounds frequently involves electrophilic aromatic substitution reactions. The conventional acid catalysts like HCl, H_2SO_4, $AlCl_3$, $ZnCl_2$, and $FeCl_3$ are required in stoichiometric ratio to carry out such reactions [2]. The use of these catalysts leads to many limitations concerning handling, safety, corrosion, and waste disposal. The development of efficient methods for recovery and reuse of the catalysts is very important in chemistry. One solution is to heterogenize the homogeneous catalysts by supporting them onto solid supports, thus providing facile recovery from the reaction mixture and the possibility of reusing them. Furthermore, Active components supported on a solid material, the surface area increases effectively and subsequently enhance the reactivity of the catalysts.

Heteropoly acid (HPA) compounds are known to be active catalysts for many acid catalyzed reactions. HPA compounds have attracted increasing interest due to their high acidity, redox properties, pseudo–liquid behaviour, physico–chemical properties, and catalytic activity. HPAs have very strong Brønsted acidity, approaching the super acid region, high stability, and high proton mobility. The Hammett acidity (H_0 = -13.2) of tungstophosphoric acid is much stronger than 100% sulfuric acid (H_0 = -11.94). Heteropoly compounds with a Keggin structure are the most studied in the polyoxometalate class because they possess relatively high thermal stability and high intrinsic acidity [3,4]. Among the Keggin type HPAs, tungstophosphoric acid

(TPA) is the usual catalyst of choice because of its high acidic strength and relatively high thermal stability. The main disadvantages of HPAs include their low surface area and high solubility in polar solvents, especially in aqueous solutions [5]. HPAs can be made into heterogeneous catalyst by exchanging their protons with metal ions such as Cs^{+} [6], Ag^{+} [7], $Sn^{4+/2+}$ [8,9], and Sm^{3+} [10] or by supporting them onto suitable supports like silica [11], zirconia [12], niobia [13], titania [14], tin oxide [15], and zeolite [16]. Activated carbons are also recommended for impregnation of heteropoly acids due to their high surface area (>1000 m^2/g), their ability to entrap certain amounts of heteropoly acid, and due to thermal stability in a wide range of p^H [17].

Activated carbons with a high surface area and porous structure have attracted increasing interest due to their novel catalytic applications. Agricultural and forest waste materials are increasingly popular for use in lightweight hybrid materials/biocomposites, chemical and food industries, as well as in the area of catalysis. Commercial activated carbons are generally prepared from coal, wood, peat, and coconut shells [18]. The demand for novel and more efficient, low–cost, and locally available renewable materials as alternative precursors in activated carbon production has led researchers to use many agricultural and forest waste materials such as fruit stones [19], pyrolyzed coffee residues [20], pine bark [21], nutshells [22] and olive stones [23] as precursors for production of activated carbons. The pinecone is a common biomass in North America and it can be converted into activated carbon using different activation methods. Huge quantities of pine trees and cones are produced throughout the world, especially in pine plantations for paper and pulp industries. Pinecones are generally discarded or burned in winter for heat generation after seed collection. The utilization of seedless waste pinecones is great potential for the production of value added products such as activated carbon.

Chimienti *et al.* (2001) reported the impregnation of Keggin type TPA and STA on carbon for the isopropanol dehydration reaction using up to 50% [24]. Their results indicated an increase in catalyst activity with increased loading up to 30%. Timofeeva *et al.* (2004), used filamentous type carbons as supports for Dawson and Keggin type tungstophosphoric acid and tested the activity of the synthesized catalysts in a reaction of 2, 6–ditert–butyl–4–methylphenol with toluene [25]. Their results showed that the activity of supported catalysts had increased due to an increase in activity of surface protons of the catalysts. Degirmenci *et al.* (2011) used activated carbon–supported silicotungstic acid and cesium salt of silicotungstic acid catalysts for synthesis of ethyl–tert–butyl ether [26]. Park *et al.* (2012) reported the effect of coke–capture in a Pd lattice on coking resistance in carbon–supported tungstophosphoric acid catalysts for dehydration of glycerol into acrolein reaction [27]. To the best of our knowledge, the synthesis of Fe–exchanged TPA supported on AC and the detailed characterization of these catalysts and their application to benzylation reactions has not been studied.

The objective of the present work was the preparation of iron salt of tungstophosphoric acid supported on activated carbon derived from pinecone biomass and the investigation of its activity for liquid phase benzylation of anisole with benzyl alcohol. The effects of the benzylating agent on benzylation of anisole and catalytic activity of the optimized catalyst compared with the activity of tungstophosphoric acid supported on activated carbon were also studied. Reaction parameters such as catalyst weight, reaction temperature, and molar ratio were optimized.

2 Materials and methods

The following analytical grade chemicals were used for catalyst preparation and benzylation of anisole reaction: Iron nitrate (Sigma–Aldrich, Canada), 12–tungstophosphoric

acid (Sigma–Aldrich, Canada), Benzyl alcohol (EM Science, Canada), dibenzylether and phosphoric acid (Alfa–Aesar, Canada), 4–methoxydiphenylmethane (Matrix Scientific, Columbia), Anisole (Alfa–Aesar, Canada). Ammonia balanced with helium, hydrogen, air, and nitrogen gases were procured from Praxair Canada.

2.1 Production of activated carbon

Pinecone activated carbon was prepared according to the procedure available in the literature [28]. Pinecones were collected from the University of Saskatchewan campus, Canada. The cones were repeatedly washed with hot distilled water to remove adhering dirt and soluble impurities and dried at overnight. The cleaned and dried pinecones were grounded and sieved to particle size >350 μm for the production of activated carbon. Activated carbon was prepared in a two–step process. In the first step, twenty grams of pinecone powder was impregnated with 60 g of 85 wt% H_3PO_4 (weight ratio 1:3). The mixture was stirred and kept overnight in a 100 °C oven. In the second step, H_3PO_4 impregnated pinecone material was placed in a fixed–bed reactor and heated under inert atmosphere of nitrogen. Initially, the temperature was raised to 150 °C at a heating rate of 10 °C/min and maintained at this temperature for 1 h. Then, the temperature was increased at the same ramping rate to reach the desired activation temperature of 500 °C and maintained at the same temperature for 2 h. Thereafter, it was allowed to cool to room temperature, followed by repeated washing with distilled water until it was free of any residual phosphoric acid (up to p^H 6.8–7.0), and the product was then dried at 110 °C for 24 h. This product was denoted as activated carbon (AC).

2.2 Preparation of the iron salt of tungstophosphoric acid

The iron–exchanged 12–tungstophosphoric acid catalyst was prepared with a nominal Fe^{3+}:TPA ratio of 1:1. TPA was dissolved in distilled water and the calculated amount of

$Fe(NO_3)_3.9H_2O$ was added to this solution and the resultant mixture was kept at 60 °C, with continuous stirring. At this stage, the solid particles grew slowly in size and yellow colour precipitates were obtained. The resultant mixture was stirred for 2 h and the excess water was evaporated on a rotary evaporator. The dried catalyst was kept for further drying in hot air oven and finally calcined at 300 ºC for 2 h. This catalyst was denoted as TPA–Fe.

2.3 Preparation of iron salt of tungstophosphoric acid supported on activated carbon

Synthesis of supported metal salt of tungstophosphoric acid prepared by the method reported in the literature [29]. A series of AC–supported variants of TPA–Fe (40–80 wt%) were prepared by the impregnation method with a nominal Fe^{3+}:TPA ratio of 1:1. The typical procedure for the preparation of 40 wt% $H_3PW_{12}O_{40}$/Fe–AC catalyst is as follows: In a 100 ml round bottom flask, 1.14 g of activated carbon (AC) was stirred in 10 ml of distilled water. 50 mg of $Fe(NO_3)_3.9H_2O$ was dissolved in distilled water and subsequently added drop–wise to the activated carbon with vigorous stirring. The required amount of aqueous solution of TPA was added drop–wise to give 40 wt% TPA–Fe on AC and the reaction mixture was stirred for a further 2 h. The excess water was removed by rotary evaporator, followed by drying the obtained powder overnight in a hot air oven at 100 ºC and then calcined at 300 ºC for 2 h under nitrogen flow. The obtained catalyst is denoted as 40TF–AC. Similarly, 50–80 wt% loading of TPA–Fe on activated carbon was prepared by varying TPA–Fe content. The obtained catalysts were denoted as xTF–AC, where x represents the amount (wt%) of loading of TPA–Fe on activated carbon.

TPA supported on activated carbon catalyst also has prepared by simple impregnation method as described above without addition of $Fe(NO_3)_3.9H_2O$ and denoted this catalyst as 70T–AC to compare the efficiency of 70TF-AC.

2.4 Characterization

The Fourier transform infrared (FT–IR) spectra were recorded in the range of 400–4000 cm^{-1} wave numbers using 16 scans and a resolution of 4 cm^{-1} with a Perkin–Elmer Spectrum GX instrument, using spectroscopic grade potassium bromide (KBr) pellets.

The Raman spectra of the prepared catalysts were recorded at room temperature in the range of 100–2500 cm^{-1} using a Renishaw inVia Raman Microscope (Spectra–Physics model 163) equipped with a He/Ne laser operated at the laser diode wavelength of 785 nm. The laser spot size was approximately 1 mm with a power of 10 mW. The catalyst samples in powder form (about 5–10 mg) were spread loosely onto a glass slide below the microscope for Raman measurements.

The total acidity of the catalysts was measured by temperature programmed desorption of ammonia (TPD–NH_3) using a Quantachrome Autosorb–iQ instrument. In a typical experiment, 0.1 g of catalyst was loaded and pretreated in helium gas at 300 ºC for 2 h, then cooled to room temperature. The adsorption of NH_3 was carried out by passing a mixture of 3% NH_3 balanced He gas over the catalyst for 2 h. The catalyst was flushed in helium gas at100 ºC for 2 h to flush off the physisorbed NH_3. The TPD analysis of the catalysts was carried out in a He gas flow (30 ml/min) with a temperature ramp of 10 ºC/min. The NH_3 desorption was monitored using a thermal conductivity detector (TCD).

BET surface area of the samples was measured with a Micromeritics ASAP 2000 instrument using low temperature N_2 adsorption–desorption isotherms. Before measurement, the samples were degassed in vacuum condition at 200 ºC. The surface area was computed from the isotherms using the multi–point Brunauer–Emmett–Teller (BET) method based on the adsorption

data in the partial pressure P/P_o range from 0.01 to 0.2. The value of 0.1620 nm^2 was taken for the cross–section of the physically adsorbed N_2 molecule.

The particle size distribution of different activated carbons was measured by laser diffraction (Malvern Mastersizer S Long Bench Particle Size Analyzer, Malvern Instruments Ltd., U.K.) using the wet feeder method. The 1000 mm lens (particle size range can be measured 4.2–3480 μm) and approximately 50 mg of sample were mixed with 100 ml of water in a sample cell and analysis was performed at 2000 sweeps. The average particle size distribution was determined from 3 replicates of each sample. The polydispersity of the powder was expressed by the span value using following equation.

$$Span = \frac{D[v,0.9] - D[v,0.1]}{D[v,0.5]} \quad (205)$$

Where D(v,0.9), D(v,0.1), and D(v,0.5) are the equivalent volume diameters at 90, 10 and 50% cumulative volume, respectively. The particle size of the primary powders was described by the volume mean diameter (VMD).

2.5 Benzylation reaction procedure

The alkylation reaction was performed in a 50 ml two–necked round bottom flask provided with a reflux condenser and nitrogen inlet. In a typical run, anisole (10 g) and benzyl alcohol (3.37 g), and catalyst (0.1 g) were placed in a flask. The reactions were performed in the temperature range of 80–140 ºC and the reaction mixture was withdrawn at different intervals and then analyzed by a gas chromatography (Agilent–7890A) equipped with a stabilwax column (30 m × 0.25 mm × 0.5 μm) and flame ionization detector (Injector temperature 280 °C, detector temperature 280 °C and column temperature range was 80–240 °C at a heating rate of 20 °C/min by holding at 80 °C for 4 min. and carrier gas (He) flow rate was 2.2 mL min^{-1}). The products

were identified using the retention times of the corresponding standard sample and confirmed by GC–MS (SHIMADZU–2010) analysis.

3 Results and discussion

3.1 FT–IR spectral analysis

Figure 1 shows the FT–IR spectra of TF–AC catalysts. The characteristic bands of the heteropoly anion were observed in the finger print region (700–1100 cm^{-1}), indicating that the Keggin structure of $PW_{12}O_{40}^{3-}$ was maintained. The characteristic bands of $PW_{12}O_{40}^{3-}$ appearing at 1081, 962, 910, and 796.5 cm^{-1} correspond to ν_{as} (P–O), ν_{as} (W–O_t), ν_{as}(W–O_c–W), and ν_{as}(W–O_e–W) vibrations, respectively [15]. In the activated carbon–supported TPA–Fe catalysts, some of the characteristic Keggin bands were also observed and other bands merged with the bands corresponding to AC. In the case of catalysts prepared with lower TPA–Fe loadings, absorption bands at about 3550 and 1620 cm^{-1} were assigned to the stretching and bending vibrations of the O–H bond, respectively. From the FT–IR patterns also noticed that with an increase in TPA–Fe loading on AC, intensity of the characteristic peak of Keggin ion was also increased. FT–IR patterns of TF–AC catalysts confirmed the presence of Keggin ion in all catalysts. The spent catalyst (70TF-AC used) was analyzed by FT-IR to determine the stability of heteropoly acid after the reaction. The FT–IR spectrum of the spent catalyst Figure 1(i) clearly shows the characteristic bands of Keggin ion indicating that the TPA–Fe remains as in case of fresh catalyst and was not affected during the reaction. Retention of the Keggin ion structure on AC–supported catalysts was further confirmed by Laser Raman and XRD techniques.

3.2 Laser Raman spectroscopy

Figure 2 shows the Laser Raman spectra of pure TPA, TPA–Fe and AC–supported TPA–Fe catalysts. Pure crystalline TPA showed peaks at 1010, 990, 893, 528, 234, and 216 cm^{-1}

related to characteristic peaks of Keggin ion [10,30,31]. TPA–Fe showed a band at 1004 cm^{-1} corresponding to asymmetric vibration of W=O_t bond [8]. The Raman bands at 903 and 535 cm^{-1} ascribed to asymmetric stretching vibration of W–O_c–W (O_c–corner sharing bridging oxygen atom) and symmetric stretching vibrations of W–O_e–W (O_e–edge sharing bridging oxygen atom), respectively [30,31]. The band observed at 231 cm^{-1} corresponds to W–O–W bending mode of vibrations, which might be due to the coupling between symmetric stretching mode of W, four co–ordinated oxygen, and the bending mode of W–O–W vibrations [32]. These results indicate that the primary structure of the Keggin ion is maintained after exchanging the protons with Fe^{3+}. Activated carbon showed two strong bands at 1330 and 1595 cm^{-1} (Figure 2a) related to the D– and G– bands, respectively [33]. These two bands were observed in all activated carbon–supported TPA–Fe catalysts. The sharp Keggin ion band (1004 cm^{-1}) was observed from 60 wt% loading of TPA–Fe on activated carbon (Figure 2d). No sharp Keggin bands were observed at less than 60 wt% TPA–Fe loading on AC, which might be due to the incorporation of TPA–Fe into the pores of AC because of its high surface area (Table 1). The most intense bands are those related to AC. Intensity of the Keggin ion band (1004 cm^{-1}) also increased with an increase in TPA–Fe loading from 60 to 80%. Figure 2 shows that the D–band corresponding to AC is shifted to higher wave number in all the catalysts, indicating the strong interaction of TPA–Fe with AC. These results indicate that the Keggin ion structure of TPA–Fe was maintained even after supporting onto AC.

3.3 XRD patterns

The existence of Keggin ion was further confirmed by X–ray diffraction technique. XRD pattern of the AC (a), 70TF–AC (b), TPA–Fe (c) and TPA (d), are shown in Figure 3. AC showed two broad peaks centered at 2θ of 23.8° and 29.8°, corresponding to the graphitic basal

plane. In the case of iron salt of TPA (TPA–Fe), the characteristic peaks related to Keggin ion were shown at 2θ of 10.5°, 14.7°, 18.1°, 21°, 23.4°, 25.7°, 29.8°, 35.2° and 38.3° which confirmed that the presence of Keggin ion in Fe exchanged TPA (TPA–Fe) catalyst [34,35]. The presence of Keggin ions clearly shown in (>60%) of TPA-Fe on activated carbon in FT-IR and Raman analysis results. In order to further confirm the presence of Keggin ion structure on activated carbon supported catalysts, XRD analysis has been performed only for the 70TF-AC catalyst because it was found to be the most active catalyst with maximum conversion. The presence of characteristic peaks of the Keggin ion was observed in the 70TF–AC catalyst, indicating that the Keggin ion structure of TPA–Fe is still maintained even after being supported on activated carbon.

3.4 BET Surface area and particle size measurements

The textural properties such as surface area, pore size, and pore volume are presented in Table 1. AC showed a high surface area of 838.4 m^2/g, whereas pure TPA–Fe showed a surface area of 1.8 m^2/g. As the TPA loading increases surface area, pore diameter and pore volume all strongly decreases relative to the support, AC. It was observed that with increased loading of TPA–Fe onto AC from 40 to 80 wt%, the surface area of the catalysts was decreased. The reason being, as the TPA–Fe loading increases on AC, TPA–Fe species enters the pores of AC it decrease the pore diameter, and the average pore volume as well as the surface area.

Typical laser diffraction technique (LDT) volume–based particle diameter distributions curves are illustrated in Figure 4. All the distribution curves have a traditional bell shape and distribution of particles sizes depended on TPA–Fe loading on AC. From Figure 4, particles sizes were distributed in a wide range (10–900 μm) for AC. On the other hand bulk TPA–Fe, particle sizes are in the range of 1–50 μm. When 40 wt% of TPA–Fe impregnated on AC, the particle

size range of the catalyst was decreased to 8–300 μm (Figure 4b). Similar trend was observed for the catalysts with higher loadings of TPA–Fe and the particle size distribution range is decreasing towards lower values. The average particle size of all the powder samples was calculated in terms of span value, as discussed in the section 2.4 and span values are presented in Table 1. Span value for AC is 4.52, which is decreased upon loading of TPA–Fe. Catalyst with 60 and 70 wt% of TPA–Fe possesses high span values compared to other supported catalysts, this is due to wide range particle distribution compared to other catalysts (Figure 4). The bulk TPA–Fe also possesses high span value (4.72). However the particle size of TPA–Fe catalyst was distributed in the range of 1–50 μm only (Figure 4).

3.5 TPD of ammonia analysis

Ammonia TPD profiles are shown in Figure 5. All AC–supported TPA–Fe catalysts showed broad ammonia desorption peaks in the range of 200–400 ºC, but activated carbon showed a small desorption peak at 220 ºC, due to the low acidity of AC compared to other catalysts. When iron salt of TPA were supported onto AC, the desorption peaks shifted to higher temperatures. In the case of the 40 wt% TPA–Fe catalyst, the desorption peak shifted to 290 ºC (Figure 5b). With increased TPA–Fe loading on AC, intensity of the desorption peak also increased. Compared to other catalysts, the 70TF–AC catalyst showed a broad desorption peak and with a further increase in TPA–Fe loading, the desorption peak shifted to lower temperatures (Figure 5f). Among these, 70TF–AC catalyst was found to possess strong surface acidity strength.

3.6 Catalyst efficiency for benzylation of anisole

Both surface area and acidity of the catalysts are important for benzylation reactions. Figure 6 shows the catalytic activities of TF–AC samples for benzylation of anisole with benzyl

alcohol. The activated carbon support and TPA–Fe individually showed very low activity for the benzylation of anisole. Conversion of benzyl alcohol in the case of AC and TPA–Fe catalysts was 2.7 and 2.5%, respectively. The low catalytic activity of the TPA–Fe might be due to the low surface area of the TPA–Fe catalyst and the Fe^{3+} sites caged by microcrystallite Keggin units of heteropoly tungstate, resulting in less availability of acidic sites for reactant molecules. Since, TPA exhibits different packing arrangements as the hydration water is lost [36]. Pore size and acidity of the heteropoly acid salt can be precisely controlled by the cation content [37]. As shown in Figure 4, TPA–Fe particle sizes are in the range of 1–50 μm and average pore diameter, pore volumes of the bulk TPA–Fe is very low compared to TPA–Fe supported on AC (Table 1). Since, the particle size, pore structure and surface area are the elements of the tertiary structure and the tertiary structure is the assembly of secondary structure (which is three dimensional structure of counter ions and Keggin ion) of heteropoly acid [38]. Due to the small pore structure for TPA–Fe, the benzyl alcohol might have not been diffused through the pores. Similar type of diffusion limitations of benzyl alcohol were observed for the catalysts with microporous network (zeolites) and poor performance was reported for benzylation reaction [39–41].

Although AC possess high pore volume and pore diameter, the catalytic activity was low this is because of the low acidity of the AC, as it showed a small desorption peak in the TPD profile (Figure 5a). However, in the case of supported catalysts, the pore diameter and pore volumes are higher than that of TPA–Fe results in drastic improvement for benzylation reaction. For the TF–AC catalysts, the alkylation activity increased as a function of active component (TPA–Fe) loading on AC. With an increase in the TPA–Fe loading from 40 to 70 wt%, conversion of benzyl alcohol also has increased from 24.5 to 98%. Higher benzyl alcohol

conversion of 98% was observed when 70TF–AC catalyst was used. This might be due to the high surface area of 70TF–AC compared to TPA–Fe and monolayer coverage of the active component (TPA–Fe) on AC might be achieved at 70 wt% loading. A further increase in TPA–Fe loading (80 wt%) leads to agglomeration of the active component (BET surface area Table 1), which results in low catalytic activity. The conversion of benzyl alcohol in the case of 80TF–AC catalyst was only 65.3%. Results of the TPD of ammonia analysis also agreed with the observed catalytic activity. The catalyst with 70 wt% TPA–Fe on AC showed strong and broad desorption peaks at higher temperatures compared to other catalysts (Figure 5). The 80TF–AC catalyst desorption peak shifted to a lower temperature compared to the 70TF–AC catalyst. BET surface area analysis results also supported that the 80 wt% loading catalyst had a low surface area (Table 1). Results of the benzylation activity and selectivity towards benzylated product were correlated with the acidity of the catalysts. Catalytic activity and selectivity towards the benzylated product also increased with TPA–Fe loading and attained maximum at 70 wt% loading. A further increase in loading the selectivity of by–product dibenzyl ether also increased.

Thermal stability and structural changes of the most active catalyst (70TF–AC) were studied by treating the sample at different calcination temperatures ranging from 400–750 ºC under nitrogen flow. The catalytic activity of the catalysts was evaluated for benzylation of anisole with benzyl alcohol.

3.7 Characterization of 70TF–AC catalyst calcined at different temperatures

3.7.1 Effect of calcination temperature

Figure 7 shows the catalytic activity of 70TF–AC calcined at different temperatures (400–750 ºC). The catalyst calcined at 300 ºC exhibited higher benzyl alcohol conversion compared to the catalyst calcined at temperatures beyond 300 ºC. With an increase in the

calcination temperature from 300 to 600 °C, conversion of the benzyl alcohol was decreased from 98% to 1%. There was no conversion of benzyl alcohol for the catalyst calcined at 750 °C. In addition, selectivity towards benzylated product was also decreased. This might be due to decomposition of the Keggin units of heteropoly tungstate and/or a loss in synergy between the support and active component at higher temperatures. FT–IR, Raman, and TPD characterization techniques were employed for these catalysts to gain insight of the mechanism involved in the catalytic reactions.

3.7.2 FT–IR spectroscopy

Figure 8 shows the FT–IR spectra of 70TF–AC calcined at different temperatures between 300–750 ºC. The catalysts calcined at 300 and 400 ºC exhibited peaks owing to the Keggin ion. The catalyst calcined at 500 ºC showed sharper and more intense peaks than the catalyst calcined at lower temperatures, which might be due to a decrease in the interaction between activated carbon and metal salt of heteropoly tungstate to give aggregates of iron exchange TPA. When calcination temperature was increased to 600 and 750 ºC, the characteristic bands of the Keggin ion were disappeared, which was attributed to decomposition of the Keggin ion into its constituent metal oxides at higher temperatures [15].

3.7.3 Raman analysis

Figure 9 shows the Laser Raman spectra of the 70TF–AC catalyst calcined at 300–750 ºC. All the catalysts showed characteristic D– and G– bands related to carbon. The catalyst calcined at 300 and 400 ºC showed characteristic bands related to the Keggin ion at 1004 cm^{-1}, owing to the asymmetric stretching frequency of the $W=O_t$ bond [15], indicating retention of the primary Keggin ion structure at these temperatures. The catalyst calcined at 500 ºC showed bands at 270 cm^{-1} ascribed to the bending mode of vibration and another broad band at 783 cm^{-1}

that corresponds to W–O–W stretching mode vibrations of tungsten oxide [42]. A weak band observed at 1004 cm^{-1} corresponds to the $W=O_t$ asymmetric vibration of heteropoly tungstate. These results suggest that the Keggin ion of heteropoly tungstate decomposition began at the calcination temperature of 500 ºC. For the catalyst calcined at 600 and 750 ºC, the Keggin ion bands were diminished and showed only bands related to WO_3 activated carbon (Figure 8d&e). The Raman spectroscopy results suggest that the 70TF–AC catalyst was thermally stable upto 400 ºC. Thereafter, decomposition was observed beyond 500 ºC.

3.7.4 TPD of ammonia

The effect of calcination temperature on benzylation of anisole was studied as a function of acidity. Figure 10 shows ammonia TPD profiles of 70TF–AC catalyst calcined at various temperatures, ranging from 300–600 ºC. With an increase in the calcination temperature from 300 to 600 ºC, the intensity of the desorption peak in the range of 200–400 ºC was decreased and shifted to lower temperatures. The catalyst calcined at a lower temperature (300 ºC) showed a broader and more intense desorption peak than catalysts calcined at higher temperatures. The catalyst calcined at 600 ºC showed a narrow desorption peak and very low catalytic activity (Figure 6). This might be due to decomposition of the Keggin ion of heteropoly tungstate into its constituent metal oxides at higher temperatures.

The decrease in benzylation activity with an increase in the catalyst (70TF–AC) calcination temperature can be explained on the basis of results obtained from the FT–IR, Raman and ammonia TPD. From the FT–IR and Raman results it was concluded that Keggin ion of the TPA–Fe was stable upto 500 °C. However, a drastic change was observed in the TPD profiles of 70TF–AC catalyst calcined in the range of 300–500 °C. This was due to partial degradation of Keggin ion and loss in synergy between the support and active component with increase in

calcination temperature from 300 to 500 °C. Therefore decrease in benzyl alcohol conversion with an increase in catalyst calcination temperature can be correlated with the acidity of the catalysts. Benzyl alcohol conversion depends on acidity of the catalyst which in turn is proportional to the presence of Keggin ion structure. Conversion of benzyl alcohol was only 1% in the case of catalyst calcined at 600 °C and there was no conversion of benzyl alcohol for the catalyst calcined at 750 °C this was due to complete decomposition of Keggin ion. High benzyl alcohol conversion in the case of 70TF–AC (calcined at 300 °C) catalyst was due to synergistic effect between TPF–Fe and activated carbon, and high acidity.

3.8 Optimization of reaction parameters

Reaction parameters such as catalyst weight, reaction temperature, and molar ratio were studied in order to get optimum conversion of benzyl alcohol and high selectivity towards benzylated products.

3.8.1 Effect of catalyst weight

To optimize the reaction parameters, the benzylation of anisole was carried out by taking various amounts of catalyst, ranging from 0.05–0.2 g, as shown in Table 2. It was observed that with an increase in catalyst weight from 0.05 g to 0.1 g, the conversion of benzyl alcohol increased from 55 to 98% and with a further increase in catalyst weight to 0.15 and 0.2 g, the conversion of benzyl alcohol reached 99.5%. Maximum conversion of benzyl alcohol conversion was observed with catalyst loading of 0.1 g, but selectivity of the products varied with increased catalyst weight. With catalyst loading of 0.05 g, the selectivity ratio of *o*- to *p*- benzylated products was observed in the ratio of 31:35 and 34% of the by–product dibenzylether was observed. Whereas, with 0.2 g of catalyst loading, the *o*-:*p*- ratio was 48:50 and only 2% of dibenzylether was found.

436

437 *3.8.2 Effect of molar ratio*

438 The effect of anisole to benzyl alcohol molar ratio was studied by varying the anisole to
439 benzyl alcohol molar ratio, and the results are presented in Table 3. Conversion of benzyl alcohol
440 was 97% at a 15:1 anisole to benzyl alcohol molar ratio. When anisole to benzyl alcohol molar
441 ratio was increased to 15:5, no significant benzyl alcohol conversion was observed; whereas, at a
442 15:10 molar ratio, conversion of benzyl alcohol decreased. It was also observed that with an
443 increase in benzyl alcohol concentration, selectivity towards benzylated products was decreased
444 and the formation of by–product increased due to the dehydration reaction [43]. At higher
445 concentrations of benzyl alcohol, more benzyl alcohol molecules were available, which resulted
446 in the formation of dibenzylether.

447 *3.8.3 Effect of reaction temperature*

448 Table 4 shows the effect of reaction temperature on benzylation of anisole with benzyl
449 alcohol. When the reaction temperature was maintained at 80 ºC, the conversion of benzyl
450 alcohol was only 2%. With an increase in the reaction temperature from 80 to 100, 120, and 140
451 ºC the conversion of benzyl alcohol increased from 2 to 18, 50, and 100%, respectively.
452 Selectivity towards benzylated products also followed the same trend, with an increase in
453 reaction temperature, the yield of benzylated products also increased. When the reaction was
454 carried out at 80 ºC, the selectivity of dibenzylether was 53% and for reactions carried out at 100
455 and 120 ºC, the selectivity was 40 and 36%, respectively. At 140 ºC, no formation of by–
456 products (dibenzylether) was observed, indicating that 140 ºC is the optimum reaction
457 temperature for this reaction.

458

3.9 Effect of Fe

To investigate the effect of iron salt of TPA, catalytic activity of 70TF–AC was compared with 70T–AC (TPA supported on activated carbon without Fe), and the results are presented in Table 5. The 70TF–AC catalyst showed 98% of benzyl alcohol conversion with selectivity of 40:38 (*o*-:*p*-). 70TAC showed only 51% of benzyl alcohol conversion and selectivity towards benzylated products, *o*- and *p*- were 38 and 33%, respectively under the same experimental conditions. These results confirmed that the iron salt of TPA supported on AC was more active compared to parent TPA supported on AC. This might be due to the generation of Lewis acidic sites (Fe^{3+} ions), leading to an increase in total acidity of the 70TF–AC catalyst.

3.10 Effect of benzylating agent

The effect of benzylating agents such as benzyl alcohol, benzyl chloride, and dibenzylether were studied on benzylation of anisole. Scheme 1 shows the benzylation of anisole with different benzylating agents such as benzyl alcohol, dibenzyl ether, and benzylchloride. To know the effect of the benzylating agent, a 15:5 molar ratio of anisole to benzylating agent (benzyl alcohol or benzyl chloride) was used. To compare the benzyl alcohol and dibenzylether conversion, the amount of dibenzylether was half the moles of benzyl alcohol used in the benzylation of anisole with the benzyl alcohol reaction. Table 6 shows the experimental results of benzylation of anisole with different benzylating agents. When dibenzylether was used as benzylating agent, 40% conversion was observed at a reaction time of 2.5 h. The selectivity of *o*- and *p*- benzylated products were 20 and 18%, respectively and 2% of benzyl alcohol was obtained as a by–product. Whereas, in the case of benzyl alcohol as the benzylating agent, 98% of benzyl alcohol conversion was observed at 2.5 h of reaction time and selectivity of *o*- and *p*-

benzylated products were found to be 39 and 38%, respectively. The by–product dibenzylether was also observed with a selectivity of 21%. In the case of benzyl chloride, 100% conversion was achieved within 30 min of reaction time.

It is observed that, benzyl chloride is more active as compared to benzyl alcohol in the benzylation of anisole reaction. This is because of the –Cl group, which makes benzyl chloride more reactive than the benzyl alcohol. The major disadvantage of using benzyl chloride as a benzylating agent is that it produces HCl as a by–product. At 2.5 h of reaction time, less conversion of dibenzylether was observed as compared to benzyl alcohol, which might be due to easier adsorption of benzyl alcohol molecules on the catalyst surface than the dibenzylether molecules, as shown in the reaction mechanism (Figure 11). Conversion of the benzylating agents were found in the order of benzyl chloride > benzyl alcohol > dibenzylether.

3.11 Leaching test of the catalyst

To know the TPA–Fe leaching from the activated carbon support, the benzylation of anisole reaction was carried out and after completion of the reaction where the conversion of benzyl alcohol was 100%, the catalyst was separated from the reaction mixture by centrifugation. A calculated amount of benzyl alcohol was added to the filtrate (reaction mixture) and the reaction was carried out (without addition of catalyst) to check if there was any leaching of the active component (TPA–Fe) from the support into reaction mixture. The reaction was continued for a period of 4 h. There was no benzyl alcohol conversion, indicating that there was no leaching of the active component during the reaction and that the reaction took place on the catalyst surface.

4 Conclusions

Iron exchanged TPA supported on pinecone activated carbon catalysts were prepared with retention of the Keggin ion structure of TPA–Fe. Pure TPA–Fe catalyst did not show considerable activity, whereas supporting the TPA–Fe on activated carbon increased the catalytic activity. Benzylation of anisole activity depended on the loading amount of TPA–Fe on activated carbon (AC). With increased TPA–Fe loading on AC, catalytic activity for benzylation anisole was increased and achieved maximum conversion (98%) of benzyl alcohol for 70 wt% loading calcined at 300 °C. Benzylation activity of anisole also depended on the surface area, acid strength distribution, and total acidity of the catalysts related to the content of TPA–Fe on AC. The role of Fe was studied by comparing the activity of the 70TF–AC catalyst with the 70T–AC (catalyst without Fe). Higher benzylation activity was observed for the 70TF–AC than the one without Fe. The effect of the benzylating agent was studied by using benzyl chloride, benzyl alcohol, and dibenzylether, with the preferential order for activity as benzyl chloride > benzyl alcohol > dibenzylether. The effect of reaction parameters such as reaction temperature, catalyst weight, and anisole to benzyl alcohol molar ratio were also studied for benzylation of anisole. The catalyst was found stable throughout, with no leaching of active content (TPA–Fe) from the AC support.

Acknowledgements

The authors greatly acknowledge the Canadian Bureau for International Education (CBIE) and Canadian Commonwealth Scholarship Program–2012 for financial assistance for facilitating this research.

527

528

529 **References**

530 [1] Olah, GA: Friedel-Crafts Chemistry. Wiley, New York, 1973.

531 [2] A. Schriesheim, Friedel–Crafts and Related Reactions, ed. G.A. Olah, Interscience, London,

532 1964, vol. II, Part I, p. 447–495.

533 [3] R.S. Drago, J.A. Dias, T.O. Maier, J. Am. Chem. Soc. 119 (1997) 7702–7710.

534 [4] J.A. Dias, S.C.L. Dias, N.E. Kob, J. Chem. Soc. Dalton Trans. 3 (2001) 228–231.

535 [5] G.A. Tsigdinos, Top. Curr. Chem. 76 (1978) 1–64.

536 [6] J.S. Santos, J.A. Dias, S.C.L. Dias, F.A.C. Garcia, J.L. Macedo, F.S.G. Sousa, L.S. Almeida,

537 Appl. Catal., A 394 (2011) 138–148.

538 [7] K.T. Venkateswara Rao, P.S. Sai Prasad, N. Lingaiah, Green Chem. 14 (2012) 1507–1514.

539 [8] Ch. Ramesh Kumar, K.T. Venkateswara Rao, P.S. Sai Prasad, N. Lingaiah, J. Mol. Catal., A

540 337 (2011)17–24.

541 [9] K. Shimizu, K. Niimi, A. Satsuma, Appl. Catal., A 349 (2008) 1–5.

542 [10] Ch. Ramesh Kumar, K. Jagadeeswaraiah, P.S. Sai Prasad, N. Lingaiah, ChemCatChem 4

543 (2012) 1360–1367.

544 [11] A. Jha, A.C. Garade, S.P. Mirajkar, C.V. Rode, Ind. Eng. Chem. Res. 51 (2012) 3916–3922.

545 [12] F. Su, L. Ma, Y. Guo, W. Li, Catal. Sci. Technol. 2 (2012) 2367–2374.

546 [13] K. Srilatha, N. Lingaiah, B.L.A. Prabhavathi Devi, R.B.N. Prasad, S. Venkateswar, P.S. Sai

547 Prasad, Appl. Catal., A 365 (2009) 28–33.

548 [14] Ch. Ramesh Kumar, P.S. Sai Prasad, N. Lingaiah, J. Mol. Catal., A 350 (2011) 83–90.

549 [15] Ch. Ramesh Kumar, P.S. Sai Prasad, N . Lingaiah, Appl. Catal., A 384 (2010) 101–106.

[16] G. Bai, T. Li, Y. Yang, H. Zhang, X. Lan, F. Li, J. Han, Z. Ma, Q. Chen, G. Chen, Catal. Commun. 29 (2012) 114–117.

[17] Y. Izumi, R. Hasebe, K. Urabe. J. Catal. 84(2) (1983) 402–409.

[18] I. Salame, T. Bandosz, J. Colloid Interface Sci. 240 (2001) 252–258.

[19] D.J. Malik, V. Strelko Jr., M. Streat, A.M. Puziy, Water Res. 36 (2002) 1527–1538.

[20] V. Boonamnuayvitaya, C. Chaiya, W. Tanthapanichakoon, S. Jarudilokkul, Sep. Purif. Technol. 35 (2004) 11–22.

[21] L.A.T. Vasconcelos, C.G.G. Beca, Eur. Water Poll. Control 4 (1994) 41–51.

[22] M. Ahmedna, W.E. Marshall, A.A. Husseiny, R.M. Rao, I. Goktepe, Water Res.38 (2004) 1062–1068.

[23] A.H.E. Sheikh, A.P. Newman, H.K.A. Daffaee, S. Phull, N. Cresswell, J. Anal. Appl. Pyrol. 71(2004) 151–164.

[24] M.E. Chimienti, L.R. Pizzio, C.V. Caceres, M.N. Blanco, Appl. Catal., A 208 (2001) 7–19.

[25] M.N. Timofeeva, M.M. Matrasova, T.V. Reshetenko, L.B. Avdeeva, A.A. Budneva, A.B. Ayupov, E.A. Paukshtis, A.L. Chuvilin, A.V. Volodin, V.A. Likholobov, J. Mol. Catal., A 211 (2004) 131–137.

[26] L. Degirmenci, N. Oktar, G. Dogu, AIChE Journal 57 (2011) 3171–3181.

[27] D.S. Park, B.K. Kwak, N.D. Kim, J.R. Park, J.H. Cho, S. Oh, J. Yi, ChemCatChem 4 (2012) 836–843.

[28] M. Momcilovic, M. Purenovic, A. Bojic, A. Zarubica, M. Randelovic, Desalination 276 (2011) 53–59.

[29] A.M. Alsalme, P.V. Wiper, Y.Z. Khimyak, E.F. Kozhevnikova, I.V. Kozhevnikov, J. Catal. 276 (2010) 181–189.

573 [30] K. Mohan Reddy, N. Seshu Babu, P.S. Sai Prasad, N. Lingaiah, Catal. Commun. 9 (2008)
574 2525–2531
575 [31] E. Caliman, J.A. Dias, S.C.L. Dias, F.A.C. Garcia, J.L. Macedo, L.S. Almeida, Microporo.
576 Mesopor. Mater. 132 (2010) 103–111.
577 [32] T. Takashima, R. Nakamura, K. Hshimoto, J. Phys. Chem. C. 113 (2009) 17247–17253.
578 [33] X. Li, J. Yang, Y. Hu, J. Wang, Y. Li, M. Cai, R. Li, X. Sun, J. Mater. Chem. 22 (2012)
579 18847–18853.
580 [34] K. Jagadeeswaraiah, Ch. Ramesh Kumar, P.S. Sai Prasad, N. Lingaiah, Catal. Sci. Technol.
581 (DOI: 10.1039/C4CY00253A)
582 [35] Chowdari Ramesh Kumar, N. Rambabu, N. Lingaiah, P.S. Sai Prasad, A.K. Dalai, Appl.
583 Catal., A 471 (2014) 1–11.
584 [36] I.V. Kozhevnikov, Catalysts for Fine Chemical Synthesis: Catalysis by Polyoxometalates,
585 Vol. 2, John Wiley & Sons Inc. 2002.
586 [37] T. Okuhara, Appl. Catal., A 256 (2003) 213–224.
587 [38] N. Mizuno, M. Misono, M. Chem. Rev. 98 (1998) 199–218.
588 [39] B. Coq, V. Gourves, F. Figueras, Appl. Catal., A 100 (1993) 69–75.
589 [40] V.R. Choudhary, S.K. Jana, B.P. Kiran, Catal. Lett. 59 (1999) 217–219.
590 [41] V.D. Chaube, Catal. Commun. 5 (2004) 321–326.
591 [42] A. Mirgorodsky, M. Colas, M. Smirnov, T.M. Mejean, R.E. Mallawany, P. Thomas, J.
592 Solid State Chem. 190 (2012) 45–51.
593 [43] A.B. Deshpande, A.R. Bajpai, S.D. Samant, Appl. Catal., A 209 (2001) 229–235.
594

Table 1 Textural properties of TF–AC catalysts.

Catalyst	Avg. pore diameter (Å)	Pore volume (cm^3/g)	BET surface area (m^2/g)	Particle volume mean diameter (μm)			*Particle size span value
				D[v,0.1]	D[v,0.5]	D[v,0.9]	
AC	38.8	0.7210	838.4	23.09	90.08	430.54	4.52
40TF–AC	36.7	0.3042	313.6	16.30	52.81	171.66	2.94
50 TF–AC	34.4	0.2214	241.3	16.42	47.19	113.41	2.06
60 TF–AC	30.9	0.1547	200.1	19.24	67.83	223.54	3.01
70 TF–AC	30.6	0.0623	81.4	4.80	49.85	219.66	4.31
80 TF–AC	26.6	0.0335	49.8	4.93	36.16	102.28	2.69
TPA–Fe	17.8	0.0035	1.8	0.29	3.61	17.31	4.72

*Particle size span values calculated by using laser diffraction technique.

Table 2 Effect of catalyst concentration on conversion of benzyl alcohol.

Catalyst weight (g)	Conversion of benzyl alcohol (%)	Product selectivity (%)		
		o-	*p*-	Ether
0.05	55.3	31.0	35.0	34.0
0.10	98.0	38.4	40.1	21.5
0.15	99.5	45.3	46.5	8.3
0.20	99.4	48.0	50.0	2.0

Reaction conditions: Anisole 10 g, Benzyl alcohol 3.37 g, Catalyst calcination temperature 300 ºC, Reaction temperature 120 ºC, Reaction time 2.5 h.

Table 3 Effect of molar ratio on conversion of benzyl alcohol.

Anisole to benzyl alcohol molar ratio	Conversion of benzyl alcohol (%)	Product selectivity (%)		
		o-	*p*-	Ether
15:1	96.8	46.7	48.5	4.8
15:5	98.0	38.4	40.1	21.5
15:10	90.2	28.2	31.2	40.6

Reaction conditions: Catalyst calcination temperature 300 ºC, Catalyst loading 0.1 g, Reaction temperature 120 ºC, and Reaction time 2.5 h.

Table 4 Effect of reaction temperature on conversion of benzyl alcohol.

Reaction temperature (°C)	Conversion of benzyl alcohol (%)	Product selectivity (%)		
		o-	*p*-	Ether
80	2.1	19.1	27.6	53.3
100	18.5	26.8	33.0	40.2
120	50	30.5	33.4	36.1
140	100	49.2	50.8	0

Reaction conditions: Anisole 10 g, Benzyl alcohol 3.37 g, Catalyst loading 0.1 g, and Reaction time 1.5 h.

Table 5 Influence of Fe on benzylation of anisole activity.

Catalyst	Conversion of benzyl alcohol (%)	Product selectivity (%)		
		o-	*p*-	Ether
70TF–AC	98.0	38.4	40.1	21.5
70T–AC	51.4	32.6	38.1	29.3

Reaction conditions: Anisole 10 g, Benzyl alcohol 3.37 g, Catalyst loading 0.1 g, Reaction temperature 120º C, and Reaction time 2.5 h.

Table 6 Effect of benzylating agent on benzylation of anisole.

Benzylating agent	Conversion of benzylating agent (%)	Product selectivity (%)		
		o-	*p*-	by–product
*Benzyl chloride	100	46	54	–
Benzyl alcohol	98	37.5	39.2	21.1
dibenzylether	40	18.1	20.4	1.5

Reaction conditions: Anisole 10 g, Benzylating agent (Benzyl alcohol 3.37 g/Benzylchloride 3.95 g/dibenzylether 3.08 g), Catalyst loading 0.1 g, Reaction temperature 120 ºC, and Reaction time 2.5 h (* Reaction time 0.5 h).

Figure captions

Figure 1 FT–IR of TF–AC catalysts series (a) AC, (b) 40TF–AC, (c) 50TF–AC, (d) 60TF–AC, (e) 70TF–AC, (f) 80TF–AC, (g) TPA–Fe, (h) TPA, and (i) 70TF–AC (used).

Figure 2 Raman spectra of (a) AC, (b) 40TF–AC, (c) 50TF–AC, (d) 60TF–AC, (e) 70TF–AC, (f) 80TF–AC, (g) TPA–Fe, and (h) TPA.

Figure 3 X–ray diffraction patterns of (a) AC, (b) 70TF–AC, (c) TPA–Fe, and (d) TPA.

Figure 4 Laser diffraction technique volume based particle size distribution curves for TF–AC catalysts. (a) AC, (b) 40TF–AC, (c) 50TF–AC, (d) 60TF–AC, (e) 70TF–AC, (f) 80TF–AC, and (g) TPA–Fe.

Figure 5 Ammonia TPD profiles of (a) AC, (b) 40TF–AC, (c) 50TF–AC, (d) 60TF–AC, (e) 70TF–AC, and (f) 80TF–AC.

Figure 6 Effect of TPA–Fe loading on AC for benzylation of anisole reaction and *ortho*- (gray bar), *para*- (hatched bar), and ether (white bar) product selectivity.
Reaction conditions: Anisole 10 g, Benzyl alcohol 3.37 g, Catalyst loading 0.1 g, Reaction temperature 120 º C, and Reaction time 2.5 h.

Figure 7 Effect of calcination on conversion of benzyl alcohol and *ortho*- (gray bar), *para*- (hatched bar), and ether (white bar) product selectivity.
Reaction conditions: Anisole 10 g, Benzyl alcohol 3.37 g, Catalyst loading 0.1 g, Reaction temperature 120 ºC, and Reaction time 2.5 h.

Figure 8 FT–IR of 70TF–AC catalyst calcined at different temperature (a) 300 ºC, (b) 400 ºC, (c) 500 ºC, (d) 600 ºC, and (e) 750 ºC.

Figure 9 Raman spectra of 70TF–AC catalyst calcined at different temperature (a) 300 ºC, (b) 400 ºC, (c) 500 ºC , (d) 600 ºC, and (e) 750 ºC.

748 **Figure 10** Ammonia TPD of 70TF–AC catalyst calcined at (a) 300 ºC, (b) 400 ºC, (c) 500 ºC,
749 and (d) 600 ºC.
750 **Figure 11** Adsorption of benzyl alcohol and dibenzylether onto catalyst surface.
751 **Scheme 1** Benzylation of anisole with different benzylating agents.
752
753
754
755
756
757

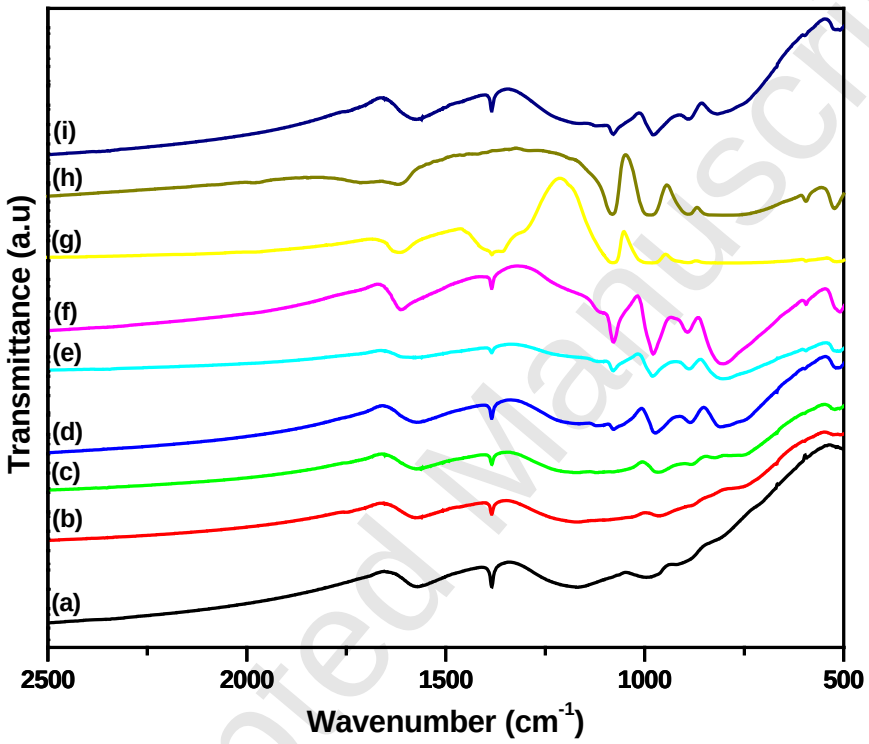

Figure 1

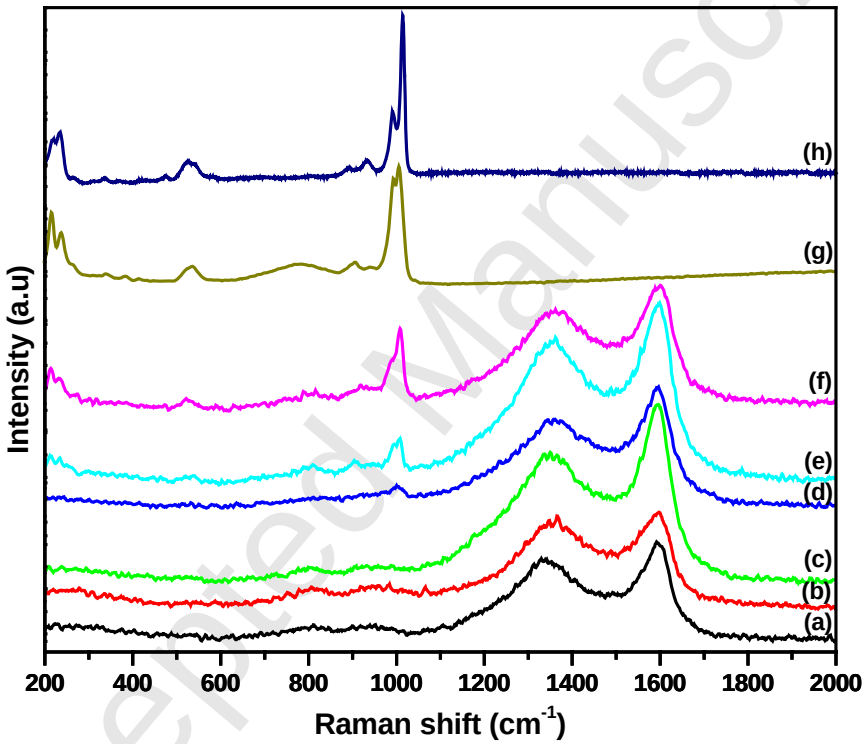

Figure 2

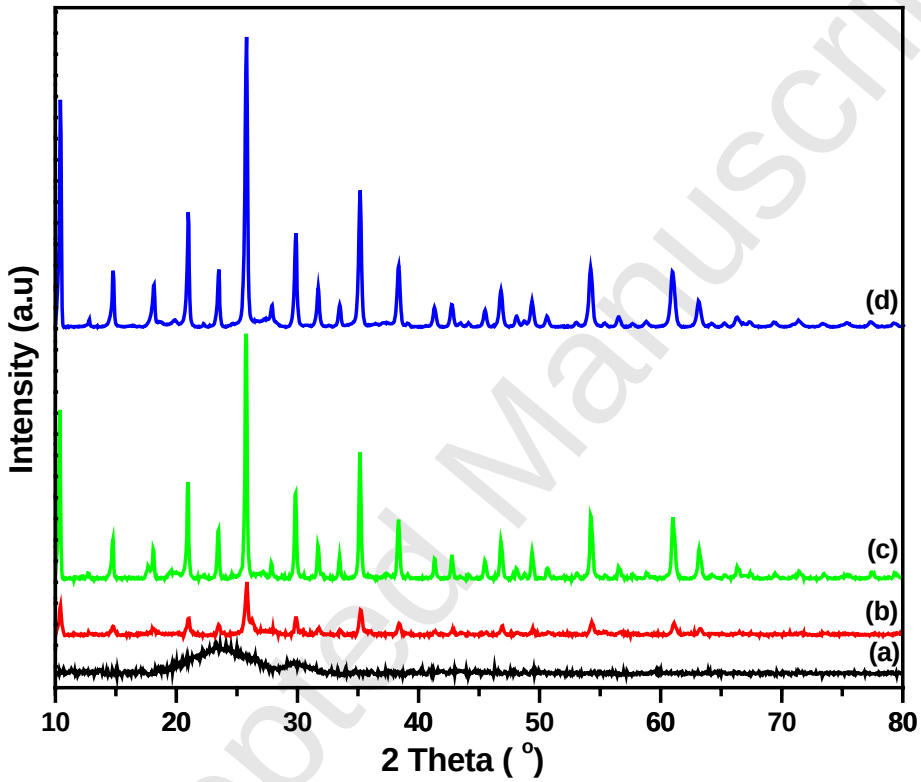

Figure 3

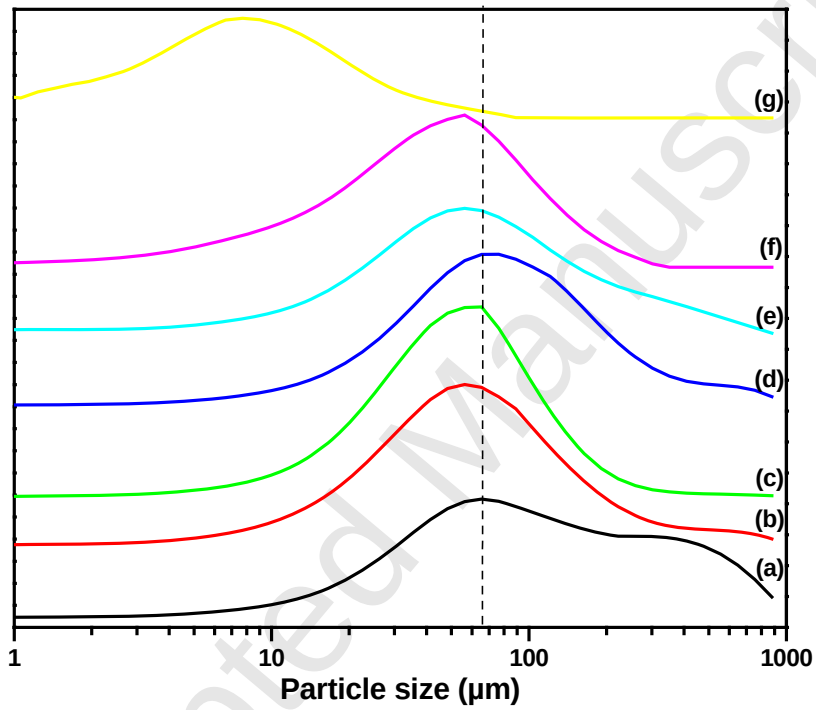

Figure 4

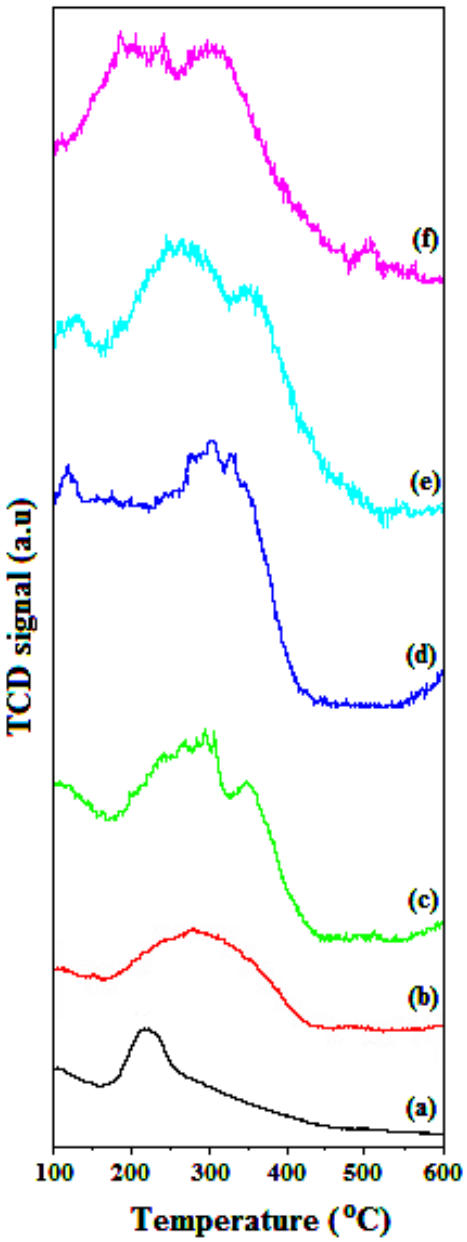

Figure 5

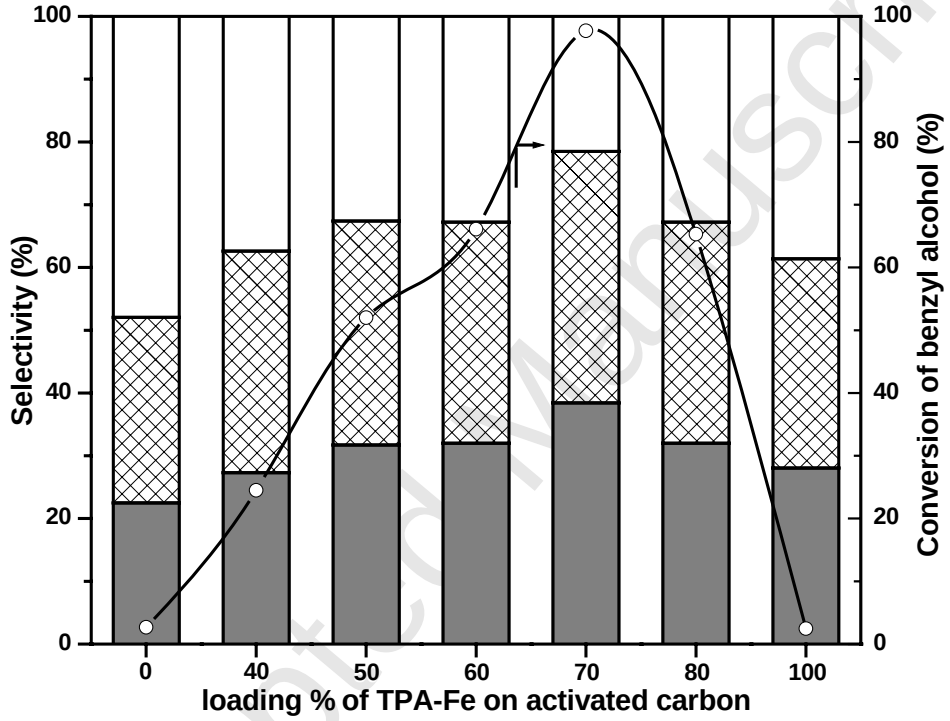

Figure 6

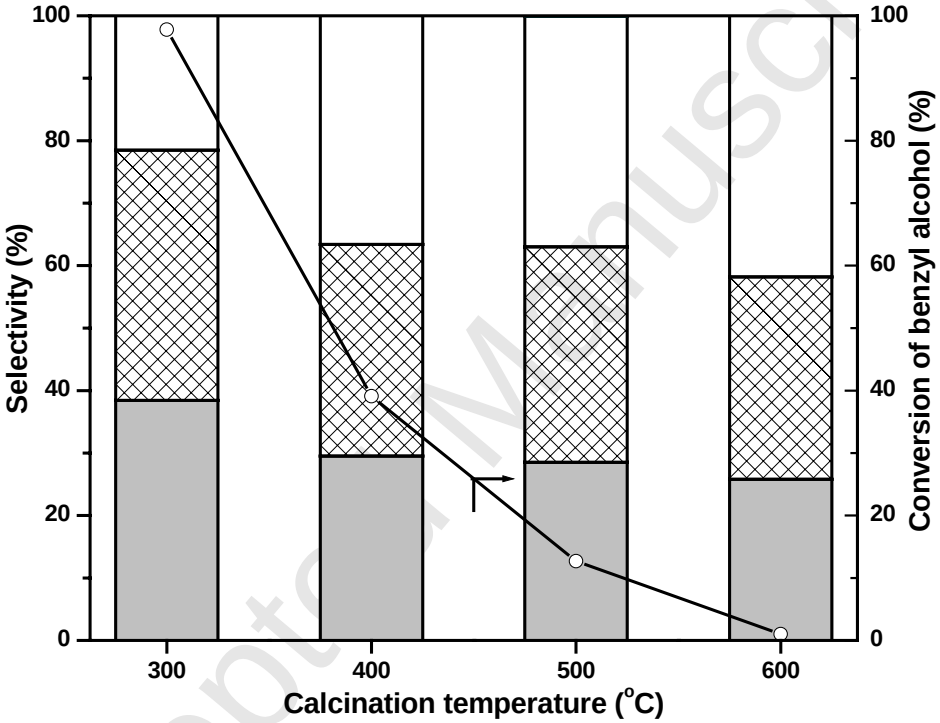

Figure 7

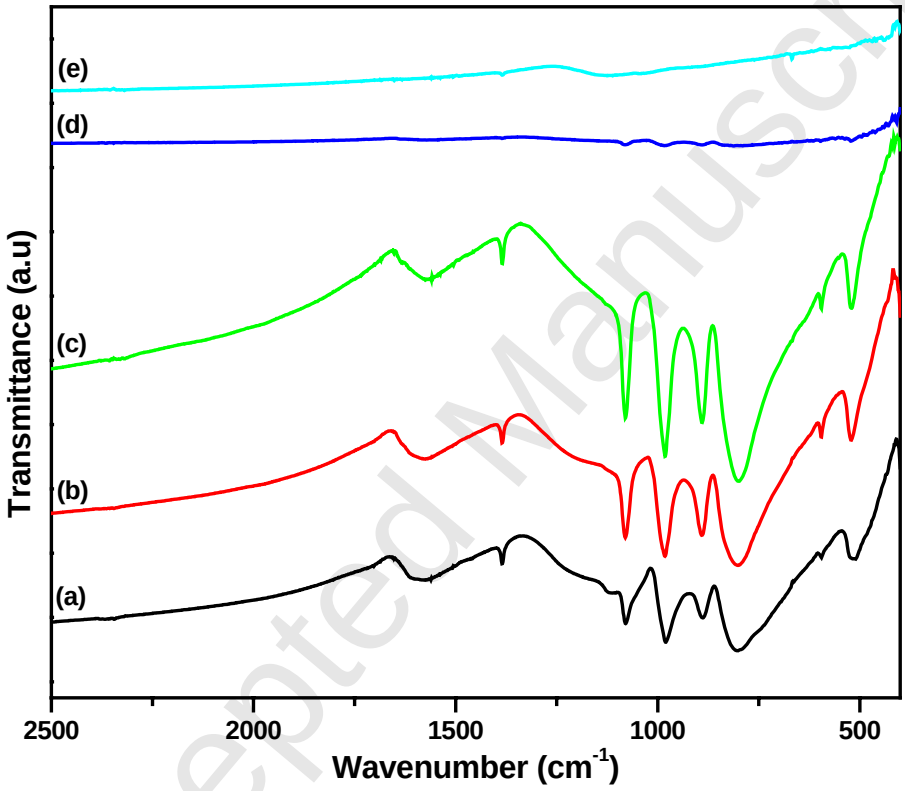

Figure 8

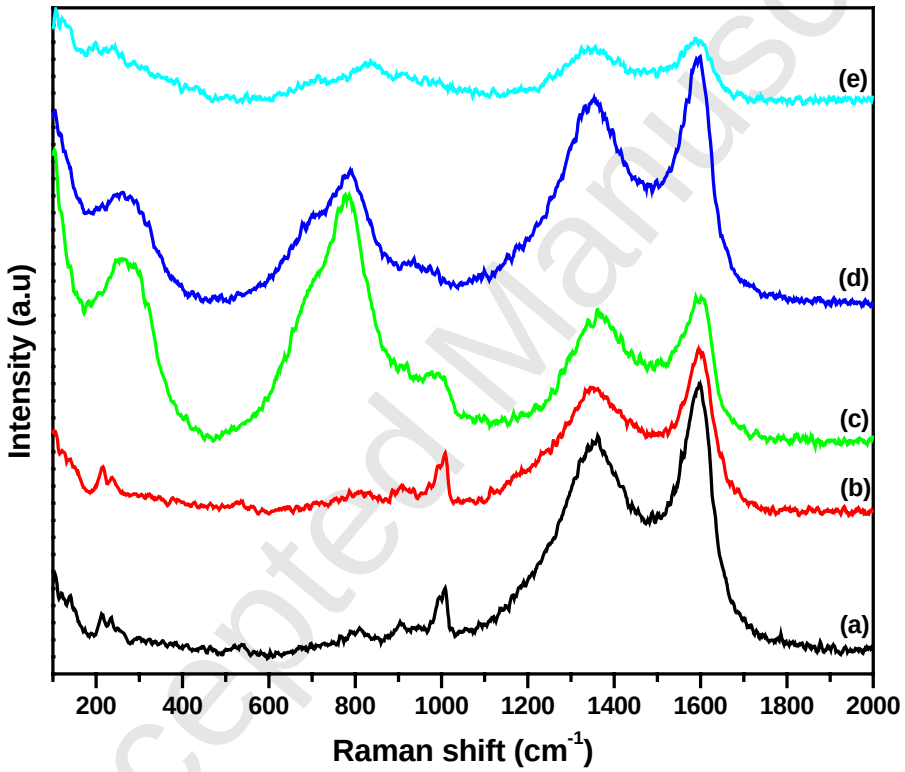

Figure 9

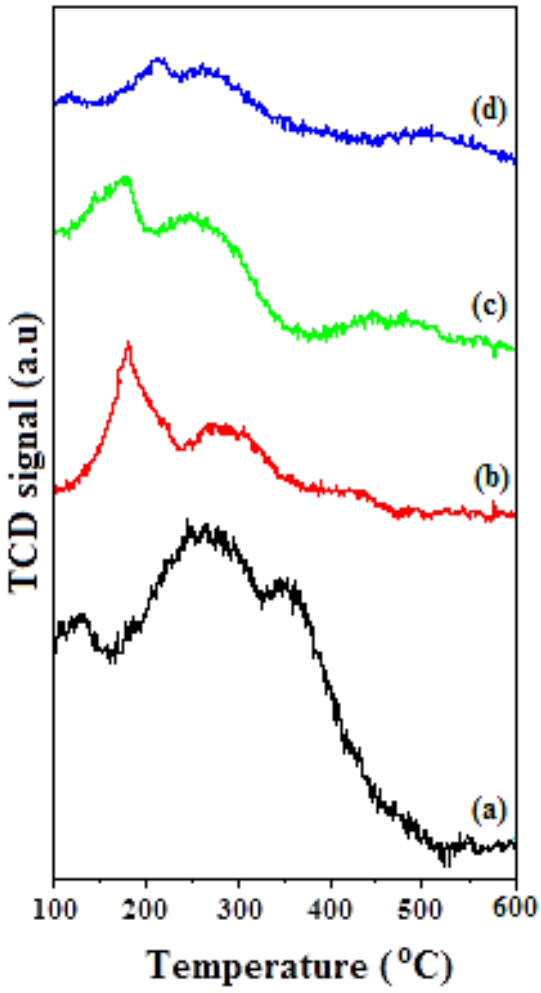

Figure 10

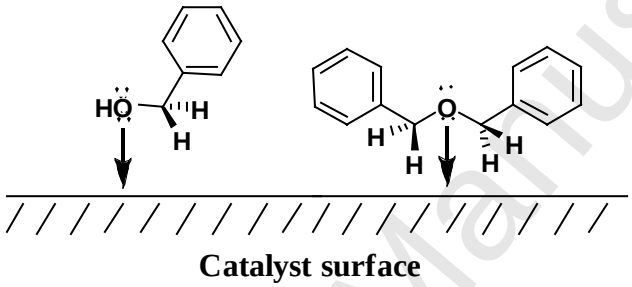

Figure 11

1096

1097

1098

1099

1100

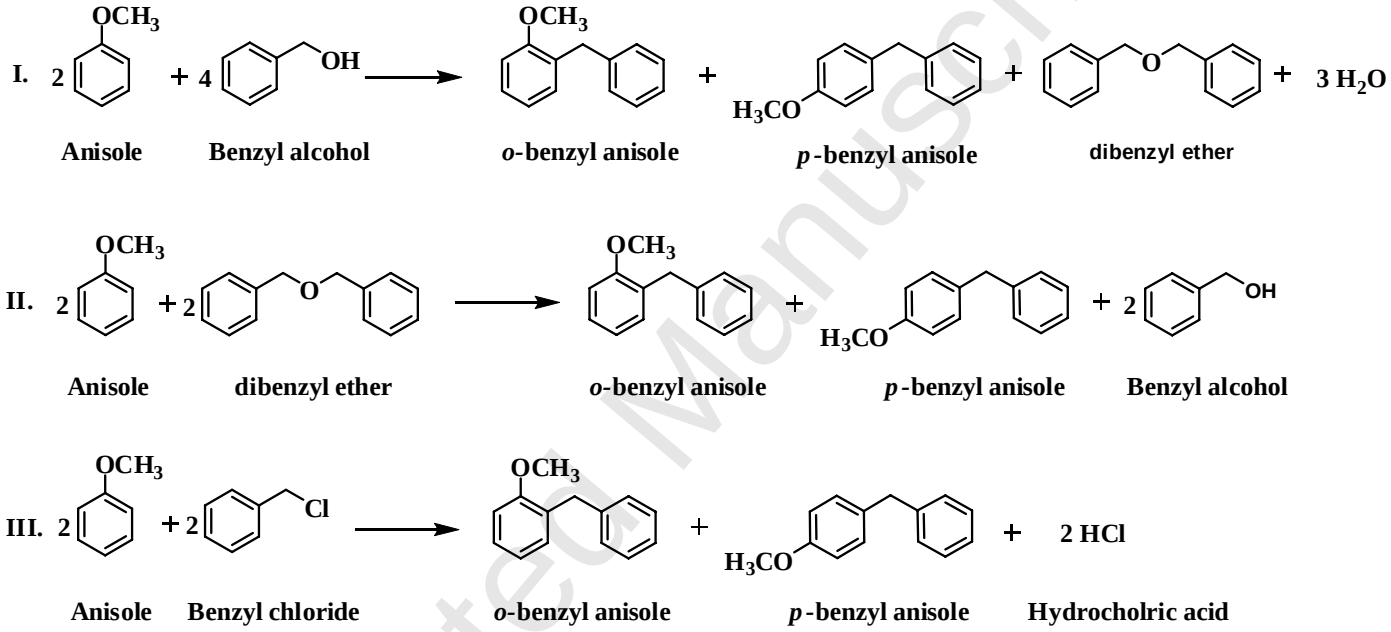

1101
1102

1103 **Scheme 1**

Graphical abstract